PROCEEDINGS OF SCIENCE

Antenna allocation technique to analyze self-generated interference

Raúl Tomás Horst,[a,b,*] **Sebastián Chiocchetti,**[b] **Nahuel Alincastro**[b] **and Daniel Lipuma**[b]

[a] *Balseiro Institute,*
Av. Bustillo km 9.5, San Carlos de Bariloche, Argentine
[b] *INVAP S.E.,*
Av. Cmte. Luis Piedrabuena 4950, San Carlos de Bariloche, Argentine
E-mail: raul.horst@ib.edu.ar, schiocchetti@invap.com.ar, nalincastro@invap.com.ar, dlipuma@invap.com.ar

This study examines how receivers can be degraded by nearby transmitters, in terms of distance and frequency, due to antenna coupling on large electrical structures. The objective is to identify methods for antenna placement to prevent self-generated interference in environments where transmitters and receivers coexist, using a communications satellite's Telemetry, Command, and Ranging (TCR) in the Ka-Band as a case study. This analysis develops a systematic approach that uses conventional computers to achieve reliable simulation within reasonable times. The work includes simulations using CST Studio Suite software, theoretical approximations, and validation through measurements to achieve the technical challenges effectively.

Radio Frequency Interference Conference (RFI2024)
14-18 October 2024
Bariloche, Argentina

*Speaker

PoS(RFI2024)051

1. Introduction

This work analyzes the potential degradation of receiver performance due to electromagnetic interference from nearby transmitters in scenarios involving large electrical structures for instance in satellites [1]. The paper aims to identify strategies for positioning antennas to prevent self-generated interference. Other key factors are the receiver's sensitivity (which varies based on the application but is typically a requirement given by the receiver's manufacturer), transmitted power, radiation patterns, and frequency bands used.

2. Modeling of large electrical structures in Ka-Band

Accurate large electrical structural modeling and appropriate simulation methods are key for obtaining reliable results efficiently with standard computing resources. Simplifications like omitting small details [2], using perfect electric conductor for conductive elements, and assuming zero thickness help reduce simulation time. Antennas should be simulated separately using time or frequency domain solvers [3]. If the separation of the antennas is smaller than the results of Equation 1 [4], the antennas are in the near-field region. If greater, they are in the Fresnel zone or far-field.

$$d = \sqrt[3]{\frac{3L^4}{\lambda}}, \tag{1}$$

where L is the maximum length of the antenna, and λ is the operational wavelength.

The integral and optical methods accept the import of near-field and far-field sources, excluding the use of other methods [3]. When using the optical method in this kind of analysis at Ka-Band, it is recommended to perform spherical ray sweeps, with steps of 0.5° in elevation and 0.01° in azimuth at least to avoid losing accuracy in the results, except in cases where the antennas are in the line of sight and it is efficient to perform a conical sweep to reduce computation time.

3. Validation

For validation purposes, the simulations are compared with corresponding measurements and a simplified mathematical model. The Friis transmission equation is introduced in Equation 2 to approximate the coupling, using the antenna geometry shown in Figure 1 [5].

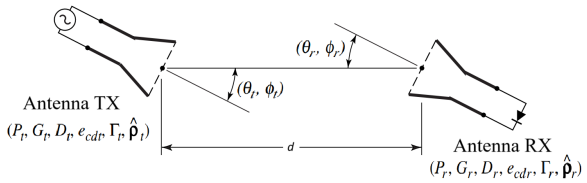

Figure 1: Geometric diagram of the transmitting and receiving antennas for the Friis transmission equation.

$$\frac{P_r}{P_t} = e_{cdt} e_{cdr} (1 - |\Gamma_t|^2)(1 - |\Gamma_r|^2) \left(\frac{\lambda}{4\pi d}\right)^2 D_t(\theta_t, \phi_t) D_r(\theta_r, \phi_r) |\hat{\rho}_t \cdot \hat{\rho}_r|^2, \tag{2}$$

where P_r is the power received by the receiving antenna, P_t is the power transmitted by the transmitting antenna, e_{cdt} is the radiation efficiency of the transmitting antenna and e_{cdr} is the radiation efficiency of the receiving antenna, Γ_t is the reflection coefficient of the transmitting antenna and Γ_r is the reflection coefficient of the receiving antenna, λ is the wavelength, d is the distance between antennas, D_t is the directivity of the transmitting antenna and D_r is the directivity of the receiving antenna, $\hat{\rho}_t$ and $\hat{\rho}_r$ are the unit polarization vectors of the transmitting and receiving antennas, respectively.

Using antennas with the same polarization, resulting in $|\hat{\rho}_t \cdot \hat{\rho}_r|^2 = 1$. The directional radiation, depending on each case, is given by $e_{cdt}(1-|\Gamma_t|^2)D_t(\theta_t, \phi_t) = G_t$, and $e_{cdr}(1-|\Gamma_r|^2)D_r(\theta_r, \phi_r) = G_r$, where G_t and G_r are the realized gains of the transmitting and receiving antennas, respectively, at the elevation angle of the employed configuration. The Equation 2 was reorganized and converted to decibels, resulting in an approximation of the coupling through Equation 3.

$$Coupling = P_r - P_t \approx G_t + G_r - 20log_{10}\left(\frac{4\pi d}{\lambda}\right). \tag{3}$$

To validate the simulation methods, the coupling between a NSI-RF-SG42 horn antenna and a WR-51 waveguide transition in the Ka-Band was measured, mounted on a structural satellite with dimensions 4.1 m (275 λ) and 1.2 m (82 λ). The horn antenna was fed through an RF generator, and the power received in the waveguide transition was measured using a spectrum analyzer. RF absorbers were used to reduce measurement errors due to unwanted reflections. Measurements were taken on the front face of the platform as a function of the distance between antennas at a height of 16.2 cm (11 λ) from the antennas at an elevation angle of 0° (aligned), as shown in Figure 2a, and also at a height of 23.2 cm (15.5 λ) with an elevation angle of 90°, as shown in Figure 2b.

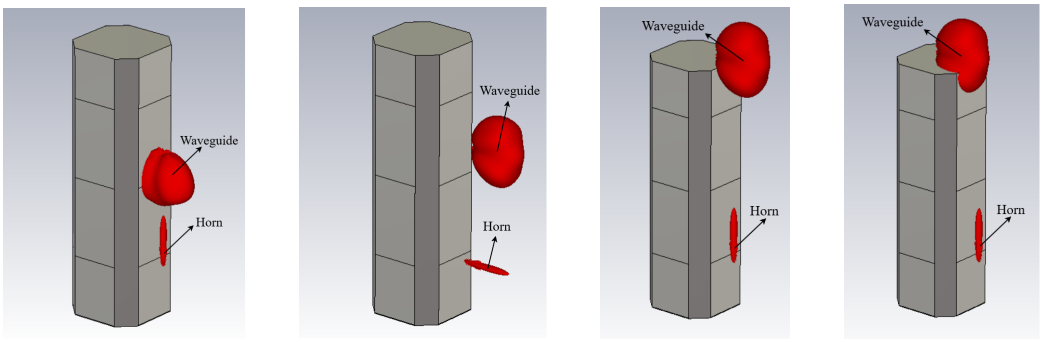

(a) Antennas height = 16.2 cm, $\theta = 0°$.

(b) Antennas height = 23.2 cm, $\theta = 90°$.

(c) Configuration referred to as case A.

(d) Configuration referred to as case B.

Figure 2: Coupling simulation between the horn and the waveguide under study on the satellite platform at 20.1 GHz. On the same face of the satellite in (a) and (b), and in different faces in (c) and (d).

Different simulation methods, using a computer with an Intel i7-7700 processor and 32 GB of RAM, were compared against the measurements. Figures 3a and 3b present the measurements

along with the theoretical curves from Equation 3 and the simulations that best fit the measurements, performed with the integral method with near-field sources for the near-field region, and the optical method with far-field sources for the Fresnel and far-field zones. Figure 3a corresponds to the aligned configuration (0° elevation) with an antenna height of 16.2 cm, and Figure 3b corresponds to the configuration at a right angle (90° elevation) with an antenna height of 23.2 cm.

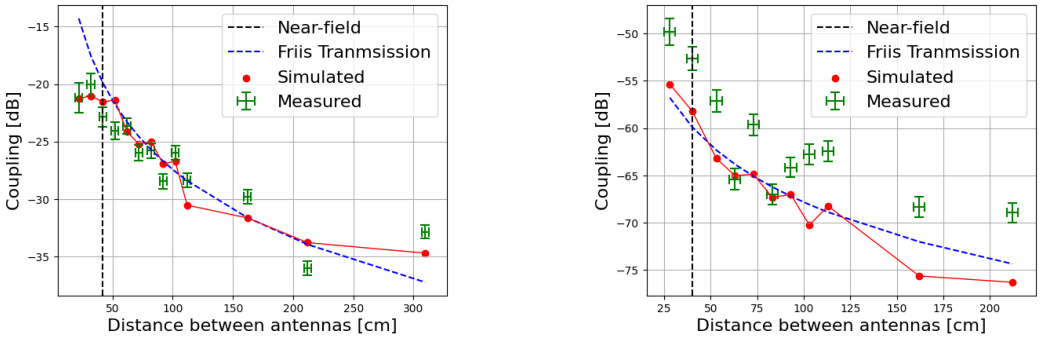

(a) Antennas height = 16.2 cm, elevation angle = 0°.

(b) Antennas height = 23.2 cm, elevation angle = 90°.

Figure 3: Coupling between the horn and the waveguide on the satellite platform as a function of distance at 20.1 GHz, at different configurations.

In addition, the coupling with the waveguide on the top face of the platform was measured in two positions, referred to as case A (Figure 2c) and case B (Figure 2d). In case A, the simulated value was -47.5 dB, and the measured value was -49.9 dB. In case B, the simulated value was -62.7 dB, while the measured value was -65.2 dB. Despite obstructing caused by the satellite platform blocking the line of sight between antennas, the optical method still accurately predicted the measured results due to the edge effects it uses to simulate the physical diffraction effect [2].

4. Results for a typical TCR

The TCR system transmits sensor data and the operational status of a geostationary satellite, and also receives control commands from the ground. Considering that the proposed analysis applies to any large electrical structure where a receiver and a transmitter coexist, a TCR mounted on a GEO satellite with a maximum dimension of 4.8 m is examined.

During the launch and early orbit phase, the TCR system uses higher powers than when the satellite is in orbit with the desired orientation, and omnidirectional antennas, as shown in Figure 4, given that the satellite is usually spinning on its axis. The frequencies of interest analyzed are 20.1 GHz, where the transmitter operates with the highest power, and 28.7 GHz, where the receiver has the highest sensitivity. The CAD model of the satellite and the far-field sources of the antennas were used to simulate the coupling between the antennas to analyze whether the received powers at the receiver comply with the interference immunity values with a safety margin of 6 dB [6]. A value of -117 dBm was obtained in the receiver at 20.1 GHz, meeting the -25 dBm interference immunity requirement and the 6 dB safety margin, and -189 dBm at 28.7 GHz, meeting the -142

dBm interference immunity mask and the 6 dB margin, ensuring that the TCR receiver will not suffer interference either at 20.1 GHz and 28.7 GHz.

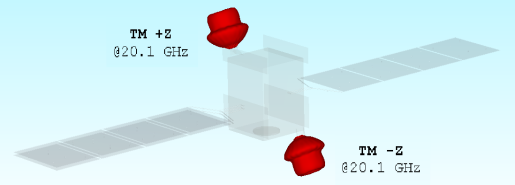

(a) Telemetry (TM) at 20.1 GHz.

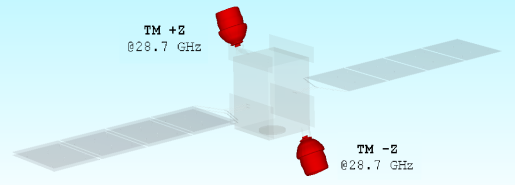

(b) Telemetry (TM) at 28.7 GHz.

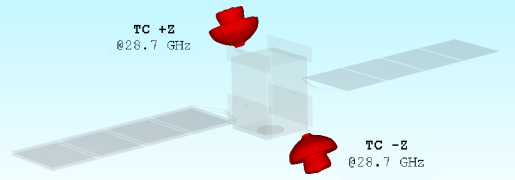

(c) Telecommand (TC) at 28.7 GHz.

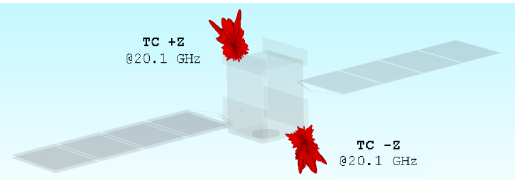

(d) Telecommand (TC) at 20.1 GHz.

Figure 4: 3D radiation pattern of the antennas used in the TCR system, mounted in the satellite.

5. Conclusions

A criterion was established to simplify the modeling of electrically large structures from an electromagnetic perspective and to define whether far-field or near-field sources are required depending on the regions of the radiation patterns, when introducing antennas into an electrical large platform. Additionally, information on the most appropriate simulation method was provided. The analysis was further optimized by providing recommendations to reduce computational resources.

The interference between the reception and transmission subsystems of a geostationary satellite's TCR was analyzed through antenna coupling simulations to evaluate the power levels received, concluding that the receiver will not suffer electromagnetic interference from the transmitter.

References

[1] R. L. L. Valle, J. G. García, and P. A. Roncagliolo, *Antenna Coupling and Out of Band Interference Effects on a High Precision GNSS Receiver*, IEEE Argentine Congress on Electromagnetism 2019, doi: 10.1109/CAE.2019.8709271.

[2] Dassault Systems, *CST Studio Suite - Antenna Placement*.

[3] Dassault Systems, *CST Studio Suite - Workflow & Solver Overview*.

[4] Trevor S. Bird, *Mutual Coupling Between Antennas.* 2021.

[5] Constantine A. Balanis, *Antenna Theory*. 4th edition.

[6] Department of Defense, USA, *MIL-STD-464C - 5.1 Margins.* 2010.